Q. J. R. Meteorol. Soc. (2001), **127**, pp. 685–708

Tropical singular vectors computed with linearized diabatic physics

By J. BARKMEIJER*, R. BUIZZA, T. N. PALMER, K. PURI and J.-F. MAHFOUF
European Centre for Medium-Range Weather Forecasts, UK

(Received 2 December 1999; revised 6 July 2000)

SUMMARY

With the introduction of diabatic processes in the forward and adjoint tangent models of the European Centre for Medium-Range Weather Forecasts's model, it is possible to determine singular vectors (SVs) for situations where diabatic physics may be important in producing perturbation growth. In this paper, the linear physical parametrizations are used to compute SVs for the tropical region, or subsets thereof, with an optimization time of 48 h. Perturbation growth is measured in terms of the so-called total energy norm, augmented with a term for specific humidity.

Difficulties that may arise in computing tropical SVs, such as associated with spurious upper-tropospheric perturbation growth, are described. Also, the impact on the SV structure by including a specific-humidity term in the defining norm is discussed. Using a term for specific humidity based on background-error statistics in the norm at initial time yields SVs with a more realistic specific-humidity vertical profile.

SVs are determined in various configurations for two tropical cyclones. Results show that targeting in the vicinity of the cyclone is required to obtain SVs associated with the cyclone dynamics. The dominant targeted SVs for tropical cyclones show resemblance to fast-growing structures found for idealized vortices.

KEYWORDS: Linear diabatic physics Numerical weather prediction Singular vectors Tropical cyclones

1. INTRODUCTION

Numerical weather prediction (NWP) models describe an intricate balance between different components of the equations of climate such as dry advective dynamics and diabatic processes like condensation and moist convection. As a consequence, the error-growth properties of an NWP model are strongly influenced by how these processes interact. Studies of the intrinsic growth of forecast errors, considering the evolution of differences between consecutive forecasts, yield error-doubling times of about 1.5 to 2 days (e.g. Lorenz 1982; Simmons *et al.* 1995). By computing so-called sensitivity fields (Rabier *et al.* 1996), or pseudo inverses of the forecast error (Gelaro *et al.* 1998), it is possible to identify fast-growing components of the analysis error. The largest possible error growth in terms of a suitable error norm during a fixed forecast period can, in principle, only be found by solving a nonlinear optimization problem. In practice, it is assumed that error growth is linear for say 2 days. Then the nonlinear optimization problem reduces to an eigenvalue problem for which efficient solvers, e.g. the Lanczos algorithm (Parlett 1980), exist.

Although the assumption of linear error growth simplifies the computation of fast-growing structures, it still requires a linearized version of the forecast model together with its adjoint because of the large dimensionality of the model. Linear models have been developed first for the adiabatic part of the forecast model, using a simplified scheme for the vertical diffusion (Buizza 1994). Although in that case the dynamics of the linear and nonlinear forecast model do not correspond precisely, they have been successfully used in various applications. In variational data assimilation, they are essential in determining the gradient of a cost function with respect to initial conditions (Thépaut and Courtier 1991; Rabier *et al.* 1997). They are also needed in the computation of singular vectors (SVs) which are used in ensemble prediction systems to create initial perturbations (Buizza and Palmer 1995; Molteni *et al.* 1996).

* Corresponding author: European Centre for Medium-Range Weather Forecasts, Shinfield Park, Reading, Berkshire RG2 9AX, UK.

Recently, linear models including moist physical processes have been developed. There is not an obvious strategy to include physical processes in the linear models, because of strong nonlinearities and the frequent dependence on logical conditionals in these processes. For a regional mesoscale model, the accuracy of the diabatic linearization is described by Vukićević and Errico (1993) and more recently by Errico and Reader (1999). They show that the accuracy depends on the atmospheric situation. Generally speaking, the match between the linear and nonlinear integrations is better over regions where geostrophically-balanced dynamics is more important than over regions dominated by convective processes. In their approach, perturbations are given a magnitude comparable with analysis uncertainties. Investigating the validity of the linear approximation in such a way is important from a practical point of view, because it reflects the actual use of SVs in ensemble prediction systems. Ehrendorfer *et al.* (1999) describe the impact of moist physics on properties as growth rate of extratropical SVs. Inclusion of diabatic processes in the linear models creates new possibilities for SVs to produce perturbation growth.

In this paper the linearized physics package of the European Centre for Medium-range Weather Forecasts's (ECMWF) global model as presented by Mahfouf (1999) is used to compute SVs. In particular, the SVs are targeted for the tropics (or subsets thereof) as defined by the longitudinal band between 30°S–30°N. This area is not yet sampled in the current ECMWF Ensemble Prediction System (EPS), because the simplified physics currently used in the SV computation (Buizza 1994) is not suitable to describe the physical processes in the tropics. The goal of the paper is to investigate the impact of moist physics on the tropical SV structure and thereby to isolate and reduce possible spurious growth mechanisms in the linearized model. In a companion paper (Puri *et al.* 2001) the impact of targeted tropical SVs, associated with tropical cyclones, on the performance of the ECMWF EPS is studied.

In defining SVs, one always faces the problem of selecting an appropriate norm to measure perturbation growth. The choice of norm depends on the particular application. For example, in the case of forecast-error covariance prediction, a norm at initial time based on the analysis-error covariance matrix is the most appropriate (Ehrendorfer and Tribbia 1997; Palmer *et al.* 1998; Barkmeijer *et al.* 1998). In this study we consider the total energy norm augmented by a term measuring specific humidity as used by Mahfouf *et al.* (1996), Buizza *et al.* (1996) and Ehrendorfer *et al.* (1999). We also experimented with a specific-humidity norm based on error variances as used in the background-error covariance matrix, operationally used at the ECMWF (Derber and Bouttier 1999).

In section 2, we briefly outline the model and linearized physics used in the SV computation. SVs and norms are defined in section 3. In section 4, examples and properties of tropical SVs are given for various settings, such as choices of the norm and target area. Special attention is given to an undesirable feature of the linearized model in creating fast-growing upper-tropospheric structures which are damped in the nonlinear forecast model. Section 5 is on tropical SVs targeted for tropical cyclones. The results are summarized in section 6.

2. THE MODEL AND SYNOPTIC SITUATIONS

The model used in this study is a low-resolution version of the ECMWF global spectral model with 31 vertical levels. In computing SVs the nonlinear model and both the linear and adjoint versions are integrated with an Eulerian advection scheme with a 20-minute time step and a triangular truncation at wave number 42. The chosen optimization time of the SVs is 48 hours. The linearized physics is the same as

described by Mahfouf (1999) and comprises vertical diffusion, subgrid-scale orographic effects, large-scale condensation, long-wave radiation and deep cumulus convection. Integrations with finite size perturbations (analysis increments) have shown that the fit between the linear and nonlinear model (using all physics) improves when physics is included in the linear model. This set of linear parametrizations is currently used in the operational ECMWF four-dimensional variational assimilation system (Mahfouf and Rabier 1999). Inclusion of physical processes increases the computational cost of SVs considerably. Apart from more memory to store additional fields during the nonlinear integration, the required computing time increases by a factor of six. A computationally demanding physical parametrization as cumulus convection which is called every time step (1200 s) contributes to almost half of this increase in computation time.

Tropical SVs targeted for the entire tropical strip were studied for two cases with forecasts starting from 12 UTC 7 February 1997 ('winter' case) and from 12 UTC 2 July 1997 ('summer' case). Also SVs were computed for two tropical cyclones. The selected cyclones were Bonnie in the Atlantic area and Zeb in the Pacific area, with forecasts starting from 12 UTC 19 August 1998 and 12 UTC 11 October 1998 respectively.

3. Singular vectors and norms

When linear perturbation growth is assumed during a certain forecast time, fast-growing structures or SVs can be determined by solving an eigenvalue problem (Lorenz 1965). Apart from an optimization time, during which perturbation growth is considered (in this study 48 hours), it is necessary to specify a norm both at initial and optimization time to measure perturbation growth. Given such norms $\mathbf{E}_0$ and $\mathbf{E}_1$, which are defined below, SVs $\mathbf{x}$ maximize the following ratio:

$$\frac{\langle \mathbf{PMx}, \mathbf{E}_1\mathbf{PMx}\rangle}{\langle \mathbf{x}, \mathbf{E}_0\mathbf{x}\rangle}. \tag{1}$$

Here $\langle\ ,\ \rangle$ denotes the Euclidean inner product $\langle \mathbf{x}, \mathbf{y}\rangle = \sum \mathbf{x}_i\mathbf{y}_i$ and $\mathbf{M}$ is the propagator of the tangent model valid for the optimization time. The positive definite and symmetric operators $\mathbf{E}_0$ and $\mathbf{E}_1$ induce a norm at initial and final time respectively. The operator $\mathbf{P}$ is a projection operator setting a vector to zero outside a given domain, e.g. outside the band 30°S–30°N. The first SV, SV1, maximizes the ratio in Eq. (1), the second SV, SV2, maximizes this ratio in the subspace $\mathbf{E}_0$-orthogonal to SV1, and so forth. Thus the singular vectors $\mathbf{x}$ define an $\mathbf{E}_0$-orthogonal set at initial time. The evolved SVs $\mathbf{Mx}$ form an $\mathbf{E}_1$-orthogonal set at optimization time in the domain defined in $\mathbf{P}$. Alternatively, these SVs are solutions of the following generalized eigenvalue problem

$$\mathbf{M}^\star\mathbf{P}^\star\mathbf{E}_1\mathbf{PMx} = \lambda\mathbf{E}_0\mathbf{x}. \tag{2}$$

The adjoint operators $\mathbf{M}^\star$ and $\mathbf{P}^\star$ are defined with respect to the Euclidean inner product. For $\mathbf{E}_0$ in the form of a diagonal matrix, as is the case for the norms considered in this paper, the square root of $\mathbf{E}_0$ is readily determined. Multiplying both sides of (2) to the left and right with the inverse of the square root of $\mathbf{E}_0$, allows us to reduce (2) to an ordinary eigenvalue problem. Although the operators $\mathbf{S}$ in (2), with $\mathbf{S}$ being $\mathbf{M}$, $\mathbf{P}$, $\mathbf{E}_0$ and $\mathbf{E}_1$, are not known explicitly, it is possible to evaluate $\mathbf{Sy}$ for a given input $\mathbf{y}$. This suffices for eigenproblem solvers such as the Lanczos algorithm, see, for example, Parlett (1980), to compute solutions of (2) in an efficient manner.

The norms $\mathbf{E}_0$ and $\mathbf{E}_1$ considered in this study are extensions of the so-called (dry) total energy (TE) norm, which is used at the ECMWF to compute SVs for the EPS

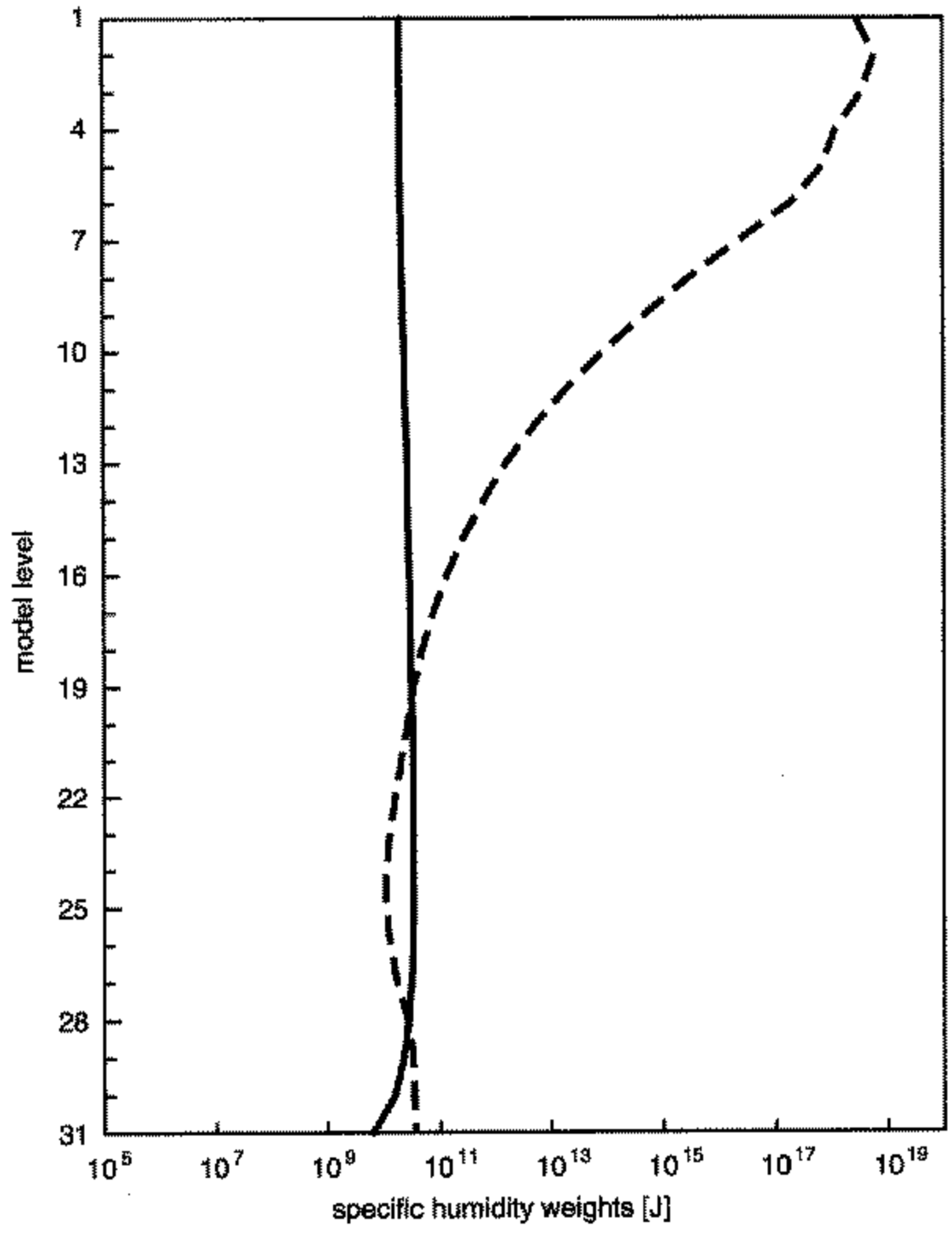

Figure 1. Weights for specific humidity as used in the standard (full line) and modified (dashed line) moist total energy norm.

(Buizza and Palmer 1995). The only difference is an additional term which measures specific humidity q. One of the norms we will consider is the moist TE-norm of which the associated inner product reads as:

$$\langle \mathbf{x}, \mathbf{E}\mathbf{y} \rangle = \frac{1}{2} \int_0^1 \int_\Sigma (\nabla \Delta^{-1} \zeta_x \cdot \nabla \Delta^{-1} \zeta_y + \nabla \Delta^{-1} D_x \cdot \nabla \Delta^{-1} D_y + \frac{c_p}{T_r} T_x T_y + w_q \frac{L_c^2}{c_p T_r} q_x q_y) \, \mathrm{d}\Sigma \left(\frac{\partial p}{\partial \eta} \right) \mathrm{d}\eta + \frac{1}{2} \int_\Sigma R_d T_r P_r \ln \pi_x \cdot \ln \pi_y \, \mathrm{d}\Sigma \quad (3)$$

with ζ_x, D_x, T_x, q_x, $\ln \pi_x$ being the vorticity, divergence, temperature, specific humidity and logarithm of the surface pressure components of the state vector $\mathbf{x}$, and c_p is the specific heat of dry air at constant pressure, $p(\eta)$ the pressure at eta levels ($0 =$ surface and $1 =$ top of atmosphere), R_d is the gas constant for dry air, $T_r = 300$ K is a reference temperature, $P_r = 800$ hPa is a reference pressure, L_c is the latent heat of condensation, and w_q is a constant.

The norm without the q term will be referred to as the dry TE-norm. When using the dry TE-norm in the SV computation, the q part of the state vector is set to zero before and after each integration of the tangent and adjoint model, see (2). The choice for the weights of the q component of the state vector in the moist TE-norm is suggested by the interaction between moisture and temperature in the condensation process when other physical processes are absent (conservation of moist enthalpy). It is assumed that the temperature T and specific humidity q of a perturbation satisfy $c_p T = -L_c q$; for more details on this see Ehrendorfer *et al.* (1999). Consequently, the temperature term in

TABLE 1. LIST OF SINGULAR VECTOR CONFIGURATIONS

Type	Physics used in linear models	q term in norm
old0 (1)	simplified physics	no (yes) at initial and final time
new0 (1)	diabatic physics	no (yes) at initial and final time
high0 (1)	as new0 but with increased vertical diffusion	no (yes) at initial and final time
qmod0	as high0	modified q weights at initial time and dry total energy norm at final time
wmod1	as high0	modified q weights at initial time and moist total energy norm at final time

(3) can be written as $c_p^2 T_x T_y/(c_p T_r) = L_c^2 q_x q_y/(c_p T_r)$. The latter expression is simply added to the dry TE-norm to define the moist TE-norm. Note that there is a weighting factor w_q in the q term. In the extreme case of $w_q \gg 1$, the dry fields will dominate at initial time, while at final time the specific-humidity field will dominate (vice versa for $w_q \ll 1$). To ensure that all components of the state vector contribute to the norm in the SV computation, both at initial and final time, a moist TE-norm with $w_q = 1$ was used, following Buizza *et al.* (1996), Mahfouf *et al.* (1996) and Ehrendorfer *et al.* (1999). This value proved to be a suitable choice for the computation of extratropical SVs. For later reference we denote SVs computed with the new linearized physics and the dry or moist TE-norm, both at initial and final time, by new0 and new1 respectively. When the linear model is used with the simplified vertical diffusion scheme as described by Buizza (1994) and currently used in the ECMWF EPS, the SVs are referred to as old0 and old1 depending on whether the dry or moist TE-norm is used. Observe that even these types of SVs may generate energy in specific humidity when integrated forward in time, simply through advection from the basic state.

We also experimented with an alternative term for specific humidity q in the moist TE-norm by using background-error statistics for q. For this we used for each model level the average error variances for q, averaged over total wave numbers, as they are specified for the operational ECMWF background-error covariance matrix (Derber and Bouttier 1999). The inverse of these averaged error variances, multiplied by a suitable factor, defines the new q weights in the modified moist TE-norm. With a multiplication factor of 5.0, the two versions of q weights are comparable for the lower part of the atmosphere; above model level 18 (500 hPa) the new q weights increase strongly. See Fig. 1 for the two versions of q weights with respect to model levels. As a reference, Table 1 summarizes the different SV configurations as defined in the paper.

4. RESULTS

We first present tropical SVs for forecasts starting from 7 February 1997 and 2 July 1997, both at 12 UTC. The optimization time used in the SV computation is 48 hours and the target area consists of the tropical band 30°S–30°N. Since the results for both the summer and winter case are often qualitatively quite similar we will mainly focus on the winter case (i.e. February 1997) hereafter.

Figure 2 shows the vorticity fields of the leading SV of type new1 for the winter (left column) and summer (right column) case at model levels 10, 11 and 12 (around 208 hPa, 238 hPa and 270 hPa respectively) at initial time. The amplitude at other model levels is negligible. The SV (especially for the winter case) has a shallow structure with amplitude concentrated at a few model levels. This is confirmed by plotting the vertical distribution of the various components of the TE-norm for SV1 as in Fig. 3 (most of the leading SVs show a similar vertical profile). The tropical SVs reveal a shallow structure

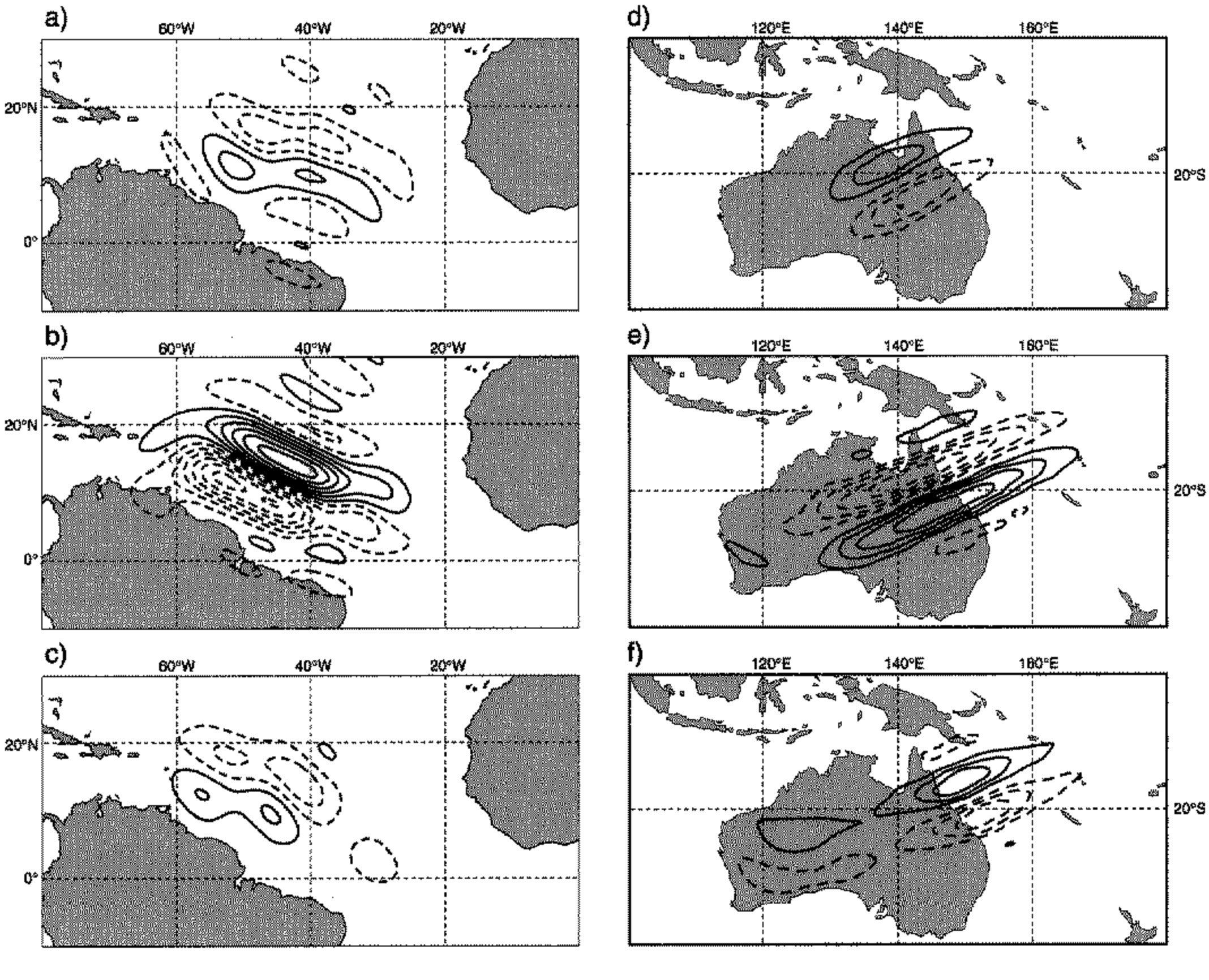

Figure 2. Left column: vorticity field of SV1 of type new1 (see text) for 12 UTC 7 February 1997 for model levels (a) 10, (b) 11 and (c) 12 (208 hPa, 238 hPa and 270 hPa respectively). Right column: same but for 12 UTC 2 July 1997. All panels use the same contour interval with negative values shown dashed.

which is entirely located in the upper troposphere and dominated by the vorticity and divergence component. Buizza and Palmer (1995) also observed a similar tropical SV structure computed with the dry TE-norm and simplified linearized physics. The vertical structure of the tropical SVs differs considerably from what is known of extratropical total energy SVs, where initially most of the energy is around 700 hPa.

Computing SVs for the different norms and using linear models with simplified and moist physics gives similar upper-tropospheric structures for the leading SVs of new0, old0 and old1 (see Table 1 for definition). The possible differences between the various types of SVs may be quantified by determining the similarity index as by Buizza (1994). In the computation of the similarity index, the unstable subspaces spanned by the leading SVs of two sets are compared by projecting one set of SVs onto another. The mean of the projection coefficients is a measure of how much the two sets of SVs differ: it ranges from 0 (for orthogonal subspaces) to 1 (for identical subspaces). In order to compare the dry and moist SVs only the dry part of the moist SV and the dry TE-norm is used in determining the projection coefficients. The results for the summer and winter cases are presented in Table 2. The upper-tropospheric SVs, which have mainly energy in the vorticity and divergence component, dominate in all types of SVs. This explains the high similarity between old0/old1 and new0/new1. Inspection of the SVs also shows that including moist processes leads to new fast-growing structures as indicated by the smaller similarity index between, for example, old1 and new1. Some of the SVs of type

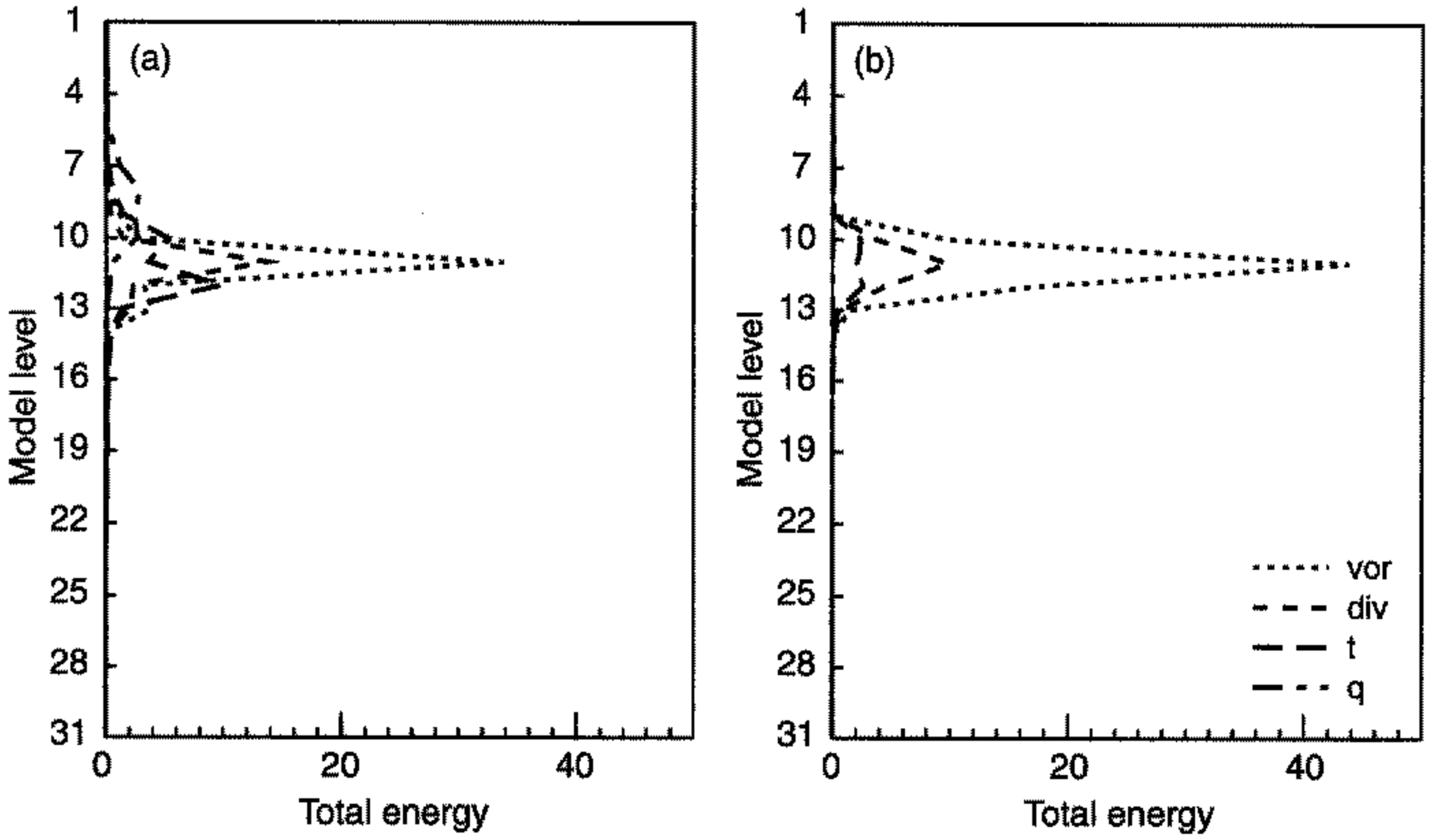

Figure 3. Vertical distribution of total energy components of SV1 of type new1 (see text) for the (a) winter and (b) summer case. Total energy is partitioned into vorticity (vor), divergence (div), temperature (t), and specific humidity (q) as shown in (b).

TABLE 2. SIMILARITY INDICES BETWEEN UNSTABLE SUBSPACES SPANNED BY THE 15 LEADING TROPICAL SINGULAR VECTORS BASED ON DRY AND MOIST NORMS (DENOTED BY SUFFIX 0 AND 1 RESPECTIVELY) AND WITH SIMPLIFIED AND NEW PHYSICS

Winter case	old0	old1	new0	new1	Summer case	old0	old1	new0	new1
old0	1	0.93	0.61	0.54	old0	1	0.75	0.56	0.48
old1		1	0.61	0.53	old1		1	0.54	0.44
new0			1	0.88	new0			1	0.82
new1				1	new1				1

new0 and new1 have resemblance to extratropical SVs. This may indicate that the target area is probably too far extended in the meridional direction to capture solely tropical error-growth mechanisms. We come back to this in subsection 4(c).

(a) *Barotropic and inertial instability*

It is not so obvious what physical mechanism is responsible for the structures as displayed in Figs. 2 and 3. It seems that baroclinic instability can be ruled out because of the shallow SV structure and the negligible contribution of available potential energy in the TE-norm at initial time, as given by the temperature component. A possible explanation may be provided by two processes which have been suggested as mechanisms for initiating tropical disturbances: inertial instability and barotropic instability (Hunt 1981; Holton 1992). In the case of inertial instability, a simple condition for instability in terms of absolute vorticity $\zeta + f$ can be derived. The inertial instability condition states that the flow is unstable in the northern (southern) hemisphere if the absolute vorticity is negative (positive). It is believed that this mechanism triggers unstable perturbations over areas with negative (positive) absolute vorticity in the northern (southern) hemisphere which reduce the lateral shear of the flow until the absolute vorticity is neutral again.

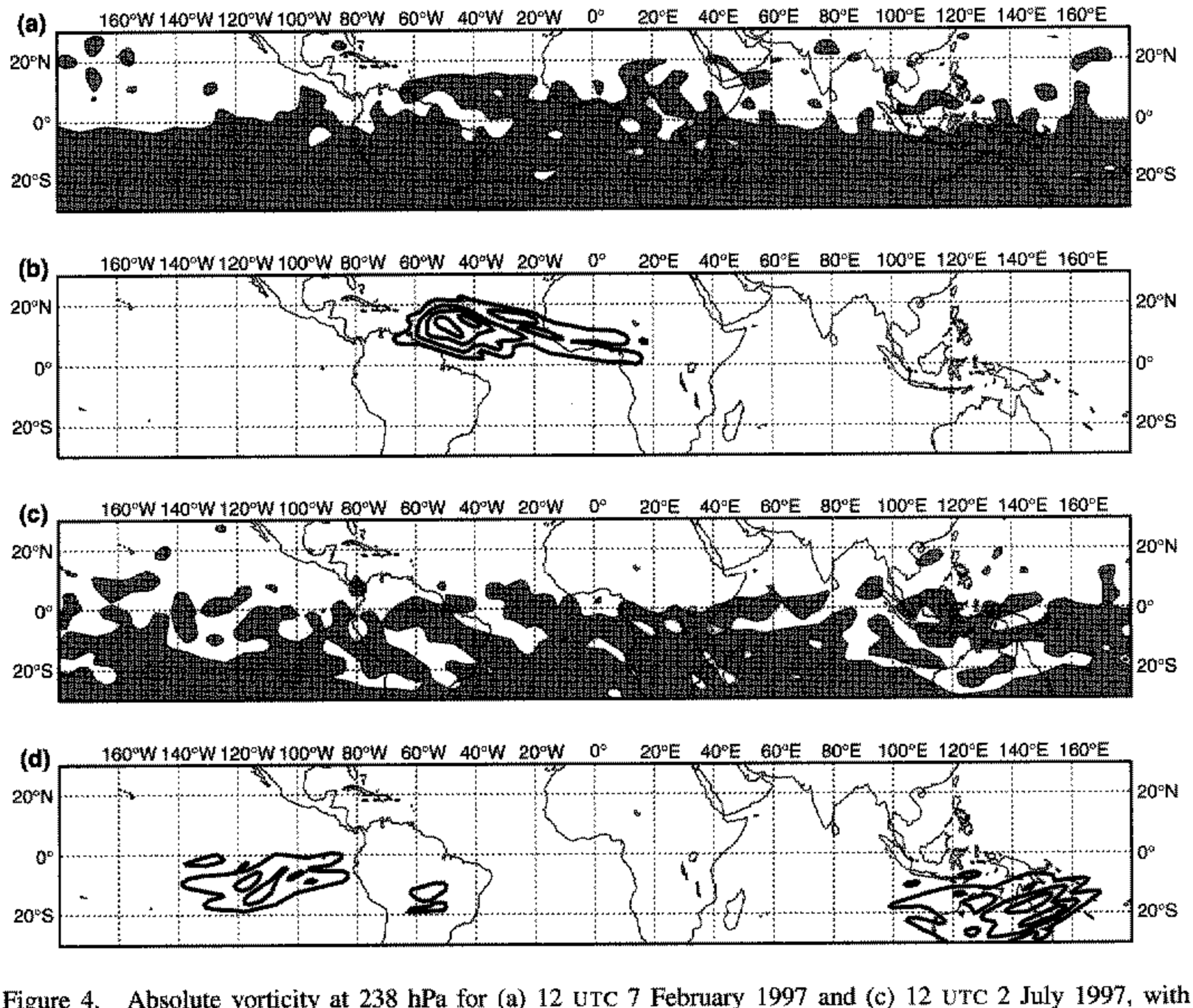

Figure 4. Absolute vorticity at 238 hPa for (a) 12 UTC 7 February 1997 and (c) 12 UTC 2 July 1997, with positive (negative) values plotted white (black). The corresponding vorticity root-mean-square fields of the 15 leading singular vectors of type new1 (see text) for both cases are given in (b) and (d) respectively.

A necessary condition for a flow to be barotropically unstable in a region is that the latitudinal gradient of absolute vorticity must vanish somewhere. To see whether the (necessary) conditions for the occurrence of these mechanisms for perturbation growth are satisfied, absolute-vorticity fields are plotted in Fig. 4. It shows for both the winter and summer case the absolute vorticity in the band 30°S–30°N of the reference trajectory at initial time for a model level where the SVs attain large amplitude. For the winter case there is a distinct area in the northern hemisphere (NH) with negative absolute vorticity extending from 60°W–30°W. The summer case is less clear, but especially the areas 140°W–20°W and 90°E–160°E in the southern hemisphere (SH) show quite a number of patches with positive absolute vorticity. It seems that the condition for inertial instability is satisfied for those areas. But, because the latitudinal gradient of the absolute vorticity also changes sign in the same areas, it may also be that barotropic instability plays a role in triggering these SVs. Therefore it is not possible to favour one of the two mechanisms for creating the large linear perturbation growth. Nevertheless, the areas indicated above seem important in defining the SVs, as can be inferred by plotting the vorticity root-mean-square fields of the 15 leading SVs (of type new1) at model level 11 for the summer and winter case. The locations of the SVs clearly match the areas related to inertial instability and barotropic instability. Particularly, the summer case nicely shows both the Pacific and South American area and the Australian area. To investigate the importance of these areas for the upper-tropospheric SVs, the

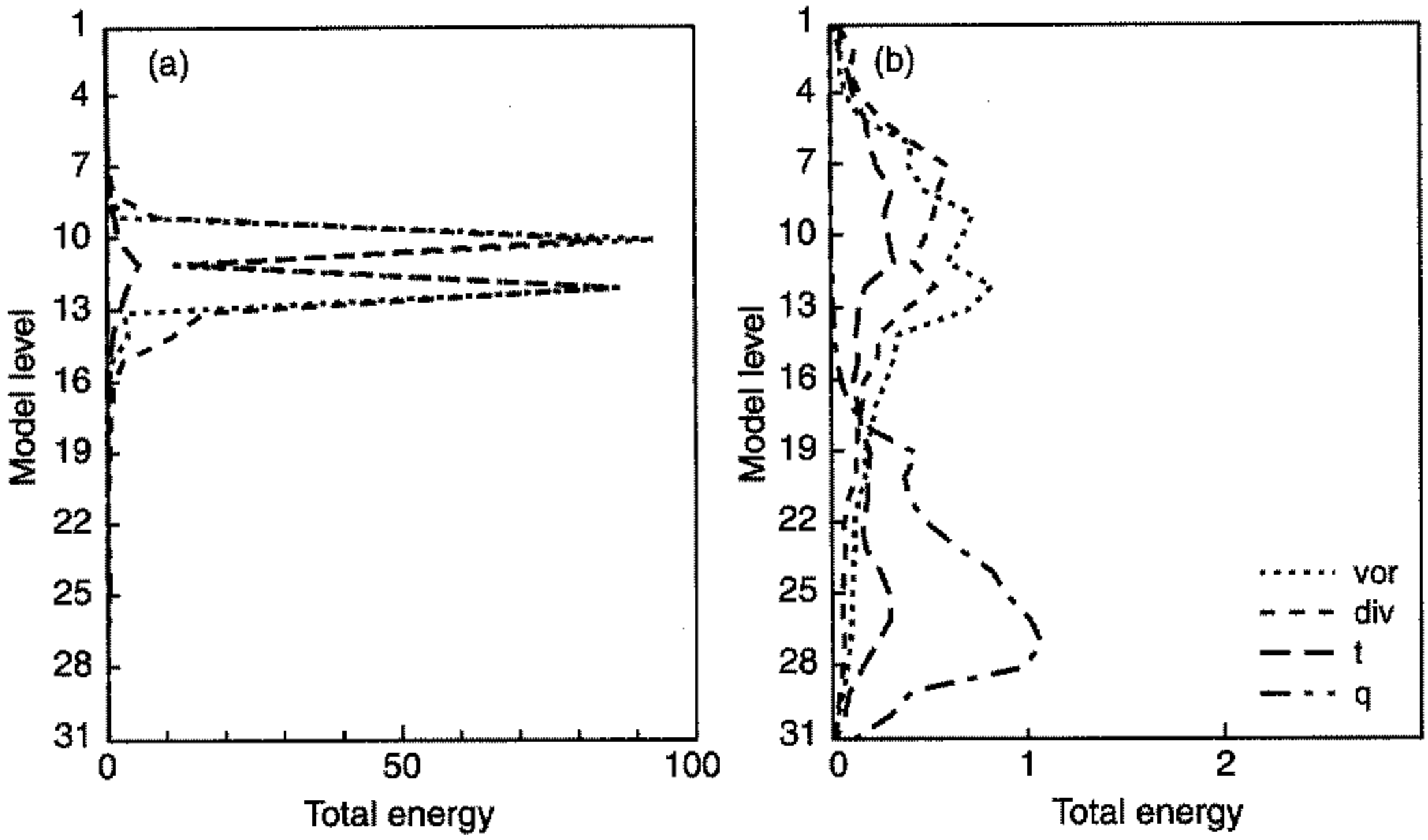

Figure 5. Energy profiles for SV1 of type new1 (winter case) (see text) after (a) linear and (b) nonlinear integrations for 48 hours. (See Fig. 3(b) for explanation of lines.)

SV computation with moist TE-norm was repeated for the winter case by excluding 70°W–50°E from the original target area. No upper-tropospheric SVs were found and the two leading SVs were identical to SV4 and SV5 of new1 (see also section 4(b)).

It is likely that these upper-tropospheric SVs are merely an artifact of the linear model, which allows for a growing mechanism absent (or much more damped) in the nonlinear model. To investigate this possible discrepancy between error-growth properties of the linear and nonlinear model, SVs (of type new1) were integrated with the same initial amplitude (or smaller) as is specified for the extratropics in the ECMWF EPS. As such, the perturbations are comparable in size (or smaller) with estimates of analysis errors. The nonlinear evolution changed the vertical structure substantially, as can be concluded from the vertical profile of the total energy distribution. In Fig. 5 the vertical energy distribution is plotted for the various components of the moist TE-norm for the linearly and nonlinearly integrated SV1 of type new1 (winter case). The large growth at the few levels, as exhibited by the linearly evolved SV1, is greatly reduced. The contribution of q, which is negligible for the linearly evolved SV, now becomes much more pronounced. Integrating SV1 nonlinearly with an initial amplitude reduced by a factor of five gave a similar energy profile as the larger nonlinear result. Reducing the initial amplitude even further did not produce the shallow structure and perturbation growth as in the linear integration. It seems that the shallow upper-tropospheric SVs are due to the linear model not being the exact tangent linear of the full model. Other SVs with not such a shallow vertical structure show a quite good correspondence between linear and nonlinear integrations.

(*b*) *Increased vertical diffusion*

The fact that the shallow upper-tropospheric SVs do not amplify in the nonlinear model indicates that they are not the signature of a genuine meteorological instability of the atmospheric flow. As a consequence, they should not be used to define initial

perturbations of the EPS. Various possibilities to avoid the growth of such SVs are examined hereafter.

Strong nonlinearities of the forward model have been identified by Mahfouf (1999) for the wind components in the tropical upper troposphere when examining the accuracy of the tangent-linear approximation (see Fig. 6 in his paper). The sharp vertical gradients of the shallow SVs can be reduced by applying the linearized vertical diffusion scheme in the upper troposphere. Such increased vertical diffusion can be regarded as an empirical way to account for damping in the nonlinear model that the linear model does not correctly represent.

The vertical diffusion scheme in the new linearized physics is based on a K-type closure with exchange coefficients depending on the local Richardson number, Ri, as described by Louis *et al.* (1982). For any conservative variable ψ (such as wind components u and v, dry static energy s or specific humidity q), the tendency of its perturbation ψ' as a result of vertical diffusion is (see also Mahfouf (1999)):

$$\frac{\partial \psi'}{\partial t} = \frac{1}{\rho}\frac{\partial}{\partial z}\left(K(Ri)\frac{\partial \psi'}{\partial z}\right) \tag{4}$$

with ρ the air density. In this linearized equation, perturbations of the exchange coefficients are not taken into account: $K' = 0$. The exchange coefficient K is defined as follows:

$$K = l^2 \left\| \frac{\partial \mathbf{V}}{\partial z} \right\| f(Ri) \tag{5}$$

where $\mathbf{V} = (u, v)$ is the horizontal wind vector and $\| \cdots \|$ denotes the Euclidean norm. The mixing-length profile $l(z)$ uses the formulation of Blackadar (1962) with a reduction in the free atmosphere expressed as:

$$l(z) = \frac{k(z + z_0)}{1 + k(z + z_0)/\lambda}\left(\beta + \frac{1 - \beta}{1 + (z + z_0/H)^2}\right) \tag{6}$$

where z_0 is the surface roughness length, k the von Kármán constant, and λ an asymptotic mixing length. The current linearized vertical diffusion scheme uses a constant pseudo height of $H = 4000$ m for the boundary layer, and a reduction factor $\beta = 0.2$ for the asymptotic mixing length in the free atmosphere.

In order to investigate the impact of increased diffusion, SVs were computed with various settings of H and β. SVs computed with a linear vertical diffusion setting with $H = 8000$ m and $\beta = 2.0$ are denoted by high1 or high0 depending on whether the moist norm is used or not. The two leading SV1 and SV2 of type high1 are identical to SV4 and SV5 of type new1 respectively as computed with the original vertical diffusion scheme ($H = 4000$ m and $\beta = 0.2$). Although, at initial time, the SVs may still extend throughout the whole depth of the atmosphere, the large amplitudes around model level 10 to 12 are now absent. SVs computed with less diffusion, e.g. $H = 8000$ m and $\beta = 1.0$, still have amplitude predominantly in vorticity and divergence and at high model levels. The fit between the linear and nonlinear evolved SVs has improved considerably with the setting $H = 8000$ m and $\beta = 2.0$. The amplification factor, defined as the square root of the ratio between the moist TE-norm in the target area of the perturbation at optimization time and the moist TE-norm at initial time, is presented in Fig. 6 for the ten leading SVs of type new1 and high1 both for linear and nonlinear integrations. Initial amplitudes were comparable with what is used in the ECMWF EPS. Clearly, the amplification factor is affected substantially by the increased

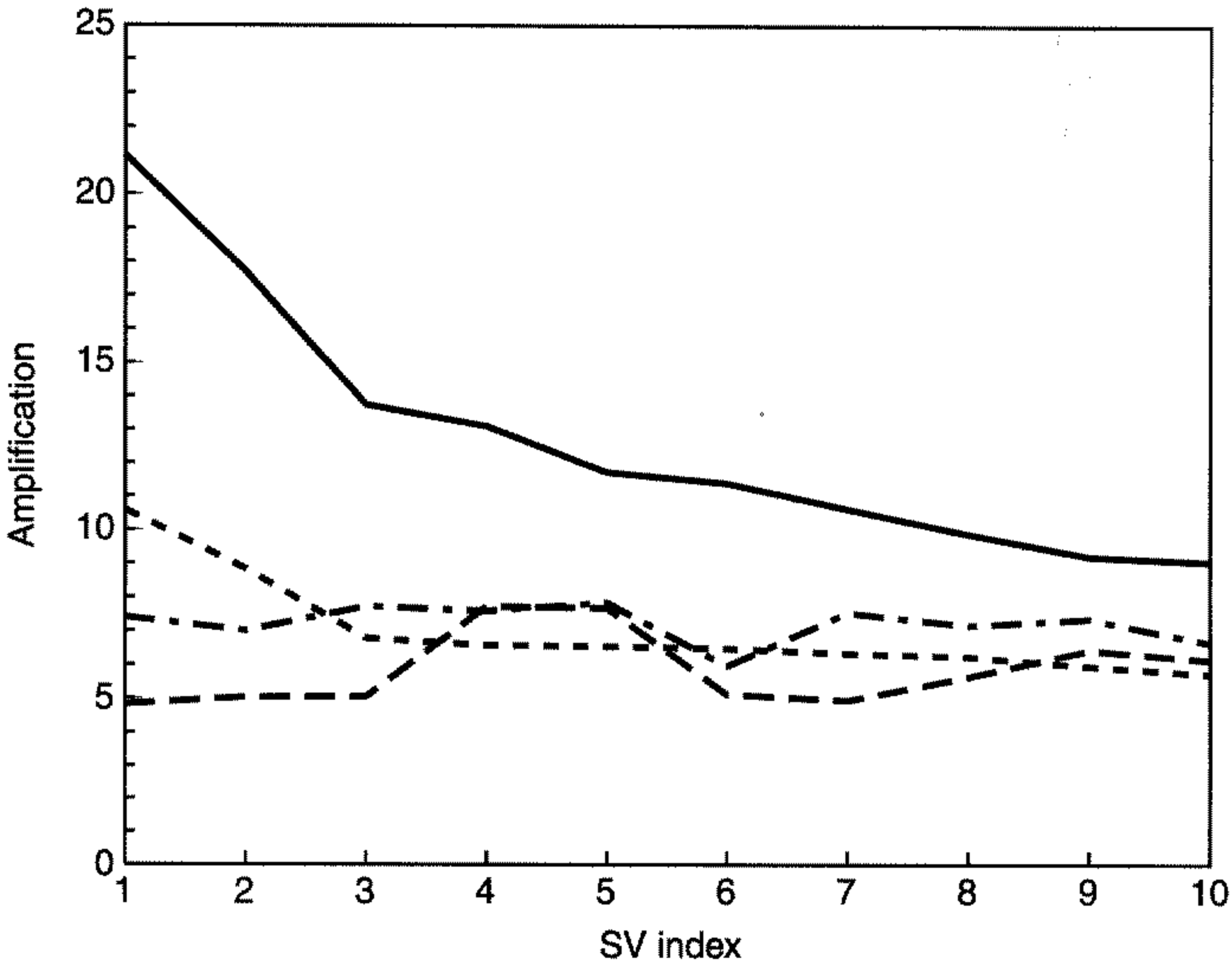

Figure 6. Total energy amplification of the ten leading singular vectors (SVs) of type new1 (winter case) as given by linear (full line) and nonlinear (long dashed) 2-day integrations and of SVs of type high1 for linear (dashed) and nonlinear (dashed-dot) integrations. (See text for further explanation.)

TABLE 3. SIMILARITY INDICES BETWEEN UNSTABLE SUBSPACES SPANNED BY THE 15 LEADING EXTRATROPICAL SINGULAR VECTORS BASED ON THE MOIST NORM AND USING SIMPLIFIED (OLD1) AND NEW PHYSICS WITH THE ORIGINAL (NEW1) AND INCREASED (HIGH1) VERTICAL DIFFUSION

Winter case	old1	new1	high1
old1	1	0.48	0.5
new1		1	0.94
high1			1

diffusion. In particular the leading SVs of type high1 yield comparable linear and nonlinear perturbation growth. Also the vertical energy profiles and spatial patterns of both linear and nonlinear integrations compare well (not shown). On the other hand, the extratropical SV computation with new physics is hardly affected by the increased diffusion.

Table 3 gives the similarity indices between three sets of extratropical SVs computed with the moist TE-norm and using simplified physics (old1), or new physics with a vertical diffusion scheme with the original parameters $H = 4000$ m and $\beta = 0.2$ (new1)

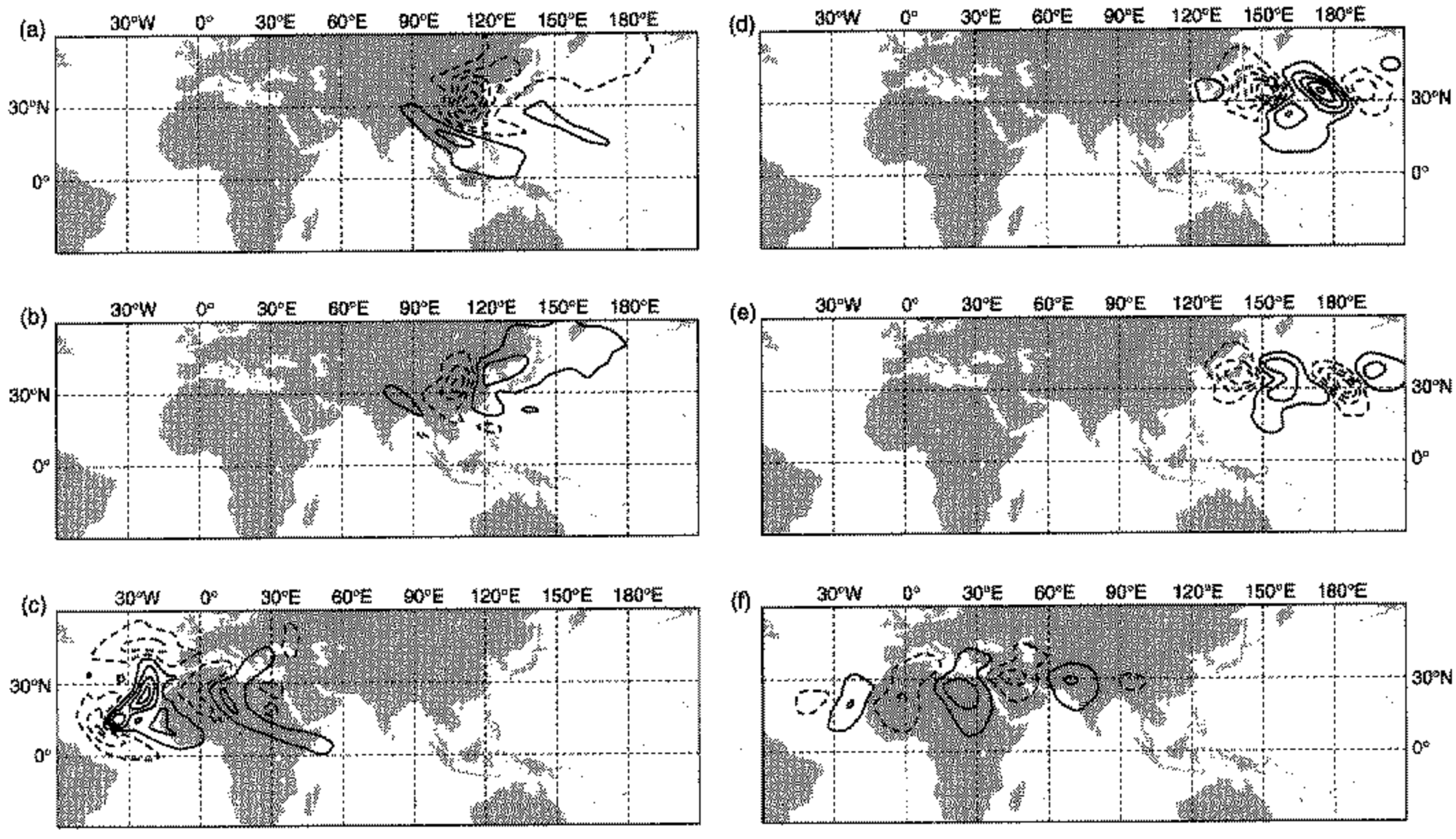

Figure 7. Stream-function fields at 500 hPa of the three leading singular vectors (of type high1 (see text) and winter case) at (a) to (c) initial and (d) to (f) optimization time. The contour interval used in (d) to (f) is a factor 20 larger than in (a) to (c). Negative values are shown dashed.

or with $H = 8000$ m and $\beta = 2.0$ (high1). The use of new physics in the tangent and adjoint models clearly leads to new structures in the subspace spanned by the leading SVs as indicated by the low similarity index with the SVs computed using simplified physics, see also Mahfouf *et al.* (1996) and Ehrendorfer *et al.* (1999). The leading SVs of type new1 yield larger amplification factors than SVs of type old1. By increasing the vertical diffusion as in high1, the amplification becomes similar to SVs of type old1 (not shown).

(*c*) *Deep tropical singular vectors*

The tropical SVs presented thus far were computed with a target area 30°S–30°N. As a consequence, SVs may have substantial amplitude in the extratropics at initial and optimization time. An example of this is shown in Fig. 7, where stream-function fields of the three leading SVs (of type high1) are plotted at 500 hPa for initial and optimization time. To ensure that the SVs are even more associated with error-growth mechanisms present in the tropics, computations were performed with a reduced target area 20°S–20°N. Unless stated otherwise, the vertical diffusion scheme with parameters $H = 8000$ m and $\beta = 2.0$ is used. It appears that the choice of target area has a substantial impact on the SV structure. The similarity index between the 15 leading moist SVs for the two target areas is only 0.23. The reduced target area yields SVs with most of the amplitude between 30°S–30°N at optimization time, and SV properties may occur which were not present for the SVs with target area 30°S–30°N. For instance, the two leading deep tropical moist SVs cannot be described by the original 15 leading moist SVs (of type high1).

The vertical energy profiles of these two SVs at initial and final time are shown in Fig. 8. Most of the total energy of SV1 at initial time is in the vorticity and temperature component and confined to the lower model levels (peaking around 800 hPa). At final time, the total energy is dominated by the specific-humidity component. This property

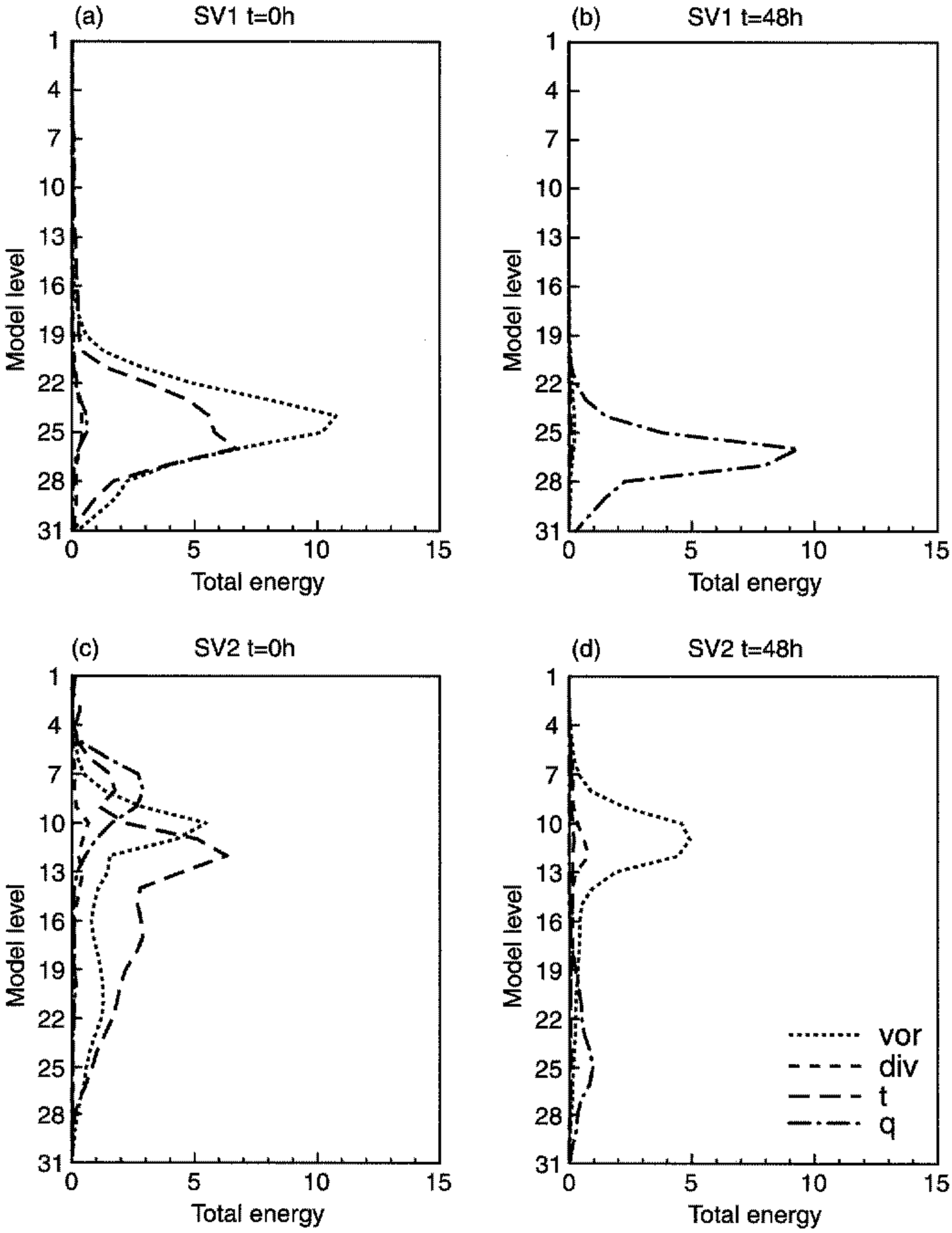

Figure 8. Energy profiles of the two leading singular vectors (SVs) of type high1 (winter case) (see text) and targeted for 20°S–20°N at (a) and (c) initial and (b) and (d) final time. The energy at initial time is multiplied by a factor of 100. (See Fig. 3(b) for explanation of lines.)

TABLE 4. SIMILARITY INDICES BETWEEN UNSTABLE SUBSPACES SPANNED BY THE 15 LEADING TROPICAL SINGULAR VECTORS FOR VARIOUS CONFIGURATIONS

Winter case	qmod0	qmod1	high0	high1
qmod0	1	0.16	0.8	0.31
qmod1		1	0.16	0.67
high0			1	0.23
high1				1

The symbol qmod0 or qmod1 denotes that the modified moist norm is used at initial time and the original dry or moist norm at final time.

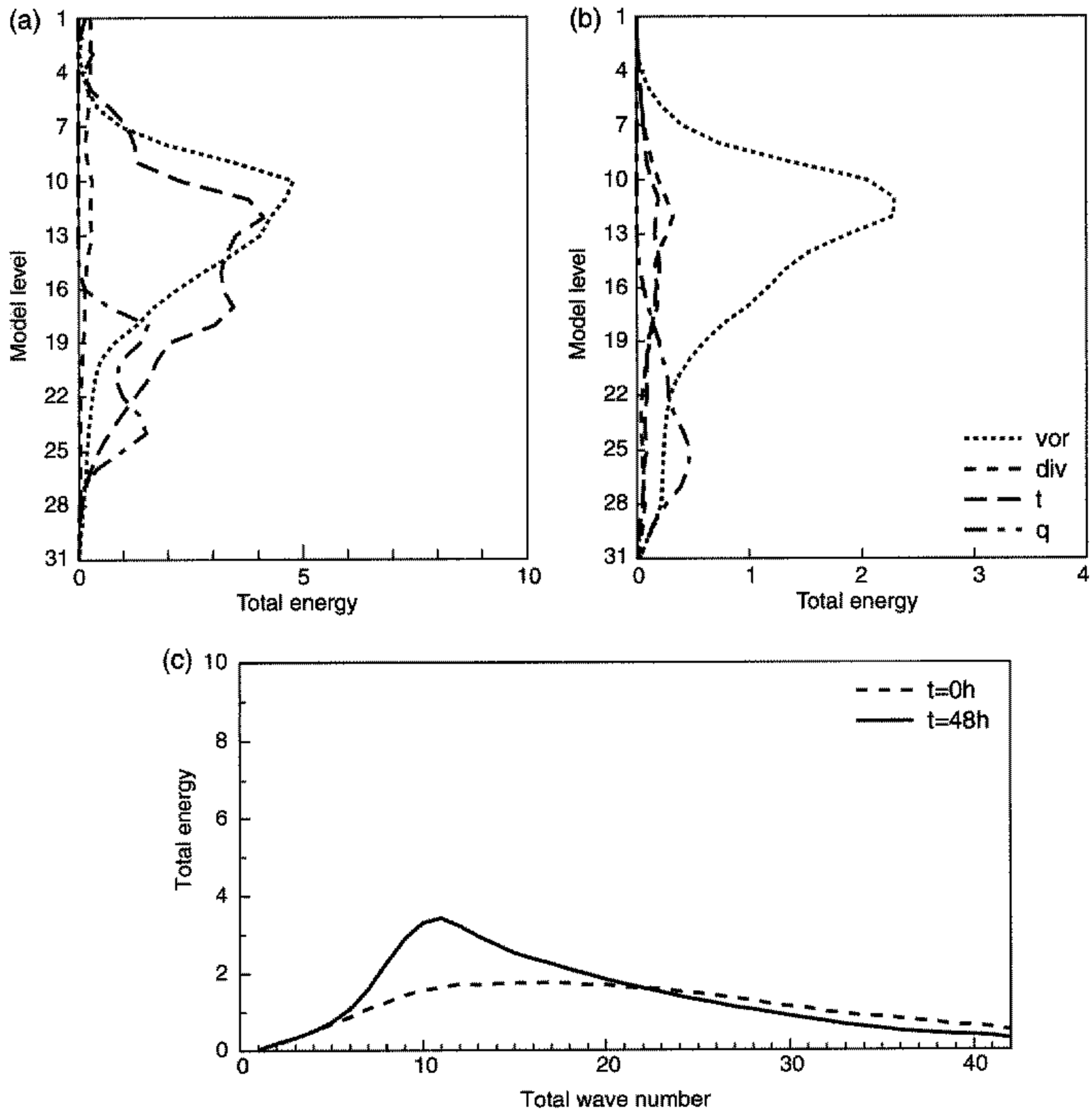

Figure 9. (a) Initial and (b) final average energy profiles for the 15 leading singular vectors (SVs) (of type qmod0 (see text) and winter case) and targeted for 20°S–20°N. (See Fig. 3(b) for explanation of lines.) (c) Corresponding horizontal energy spectra at initial (dashed line) and final (full line) time. The energy at initial time is multiplied by a factor of 100.

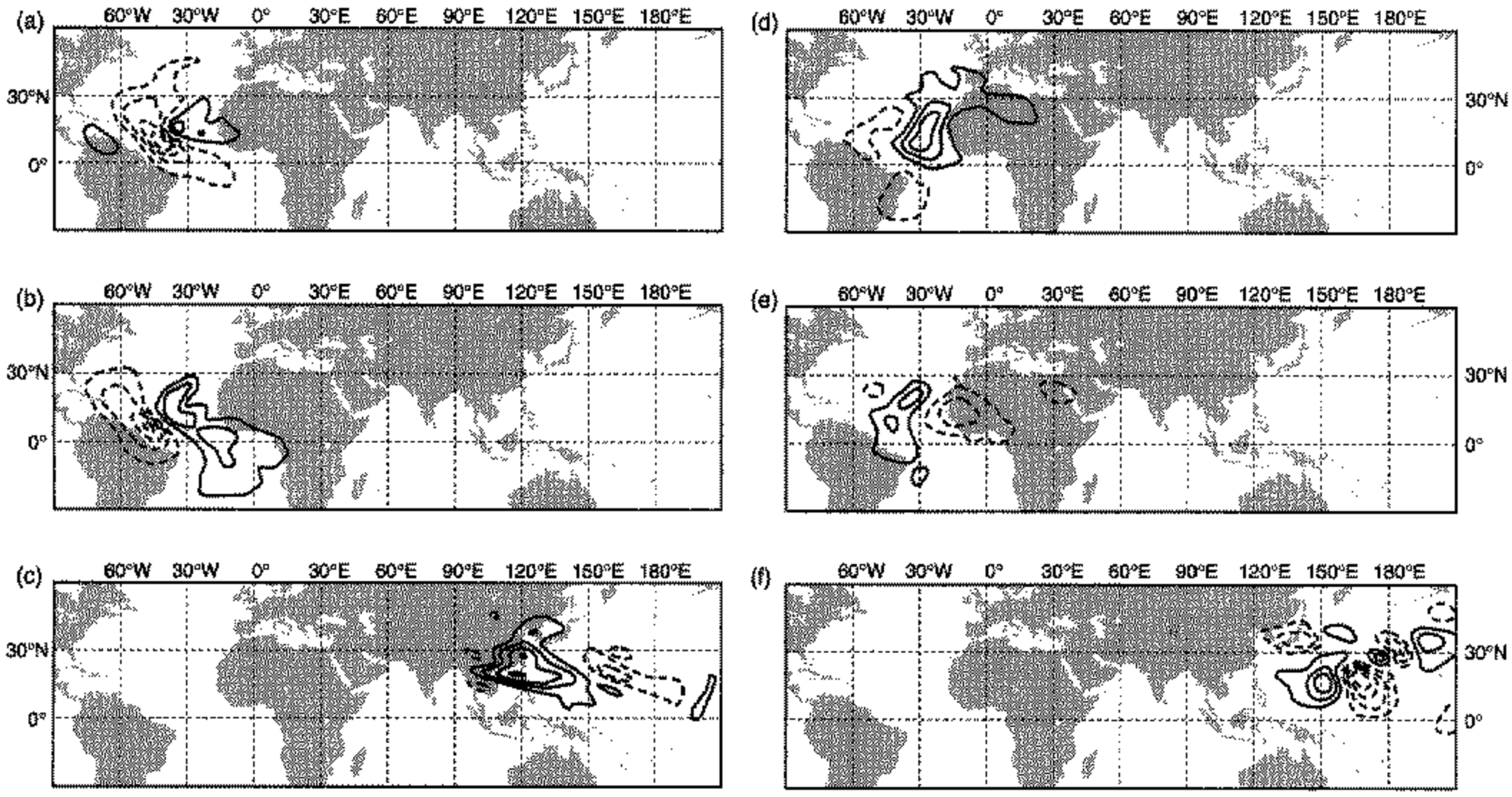

Figure 10. Stream-function fields at 500 hPa of the three leading singular vectors (of type qmod0 (see text) and winter case) and targeted for 20°S–20°N at (a) to (c) initial and (d) to (f) final time. Contour interval at final time is a factor 10 larger than used at initial time. Negative values are shown dashed.

of transforming all energy in the specific-humidity component during the 2-day linear integration occurs for most of the leading moist SVs, but is absent when the dry norm is used. Nonlinear integrations of SV1 show that this energy reversal (Ehrendorfer *et al.* 1999) is not a result of approximations in the linear models but can also occur for nonlinear evolution of such perturbations. Another SV feature which becomes apparent when computing deep tropical SVs is the vertical distribution of specific humidity at initial time. Figure 8(c) shows a large amplitude in the q term for SV2 at initial time at high model levels (peaking around 155 hPa) where the atmosphere is very dry.

To reduce the amplitude for q at high levels a modified moist norm for q was used at initial time based on background-error covariances, showing an increase in weight above model level 15 (see Fig. 1). Depending on whether the original dry or moist norm is used at final time such SVs are denoted by qmod0 or qmod1 respectively. Table 4 gives the similarity indices for various SV configurations. Clearly, use of the modified moist norm has an impact on the unstable subspace. For instance, the experiments high1 and qmod1 have a similarity index of 0.67. Inspection of the unstable subspace of qmod1 shows that, for instance, SVs like SV2 of high1 with the q profile shown in Fig. 8(a) are absent. Both computations high1 and qmod1 yield, however, several leading SVs with the energy reversal to q as shown in Figs. 8(c) and (d). Computations for other cases showed that this property is quite generic for high1 and qmod1 experiments, where q is used in the final norm. Setting the contribution of q in the final norm to zero, but allowing amplitude in q at initial time as in qmod0, yields a subspace which is quite similar (similarity index is 0.8) to the subspace obtained in high0 where the q amplitude is also set to zero at initial time. Note that the SVs of qmod0 are not ordered anymore according to their TE amplification as for the SVs in high0, because different norms are used at initial and final time.

Figures 9(a) and (b) show the mean energy profiles (averaged over the leading 15 SVs) of qmod0 at initial and final time. The upward propagation of energy, as seen in the extratropical total energy SVs, is absent. The energy profiles for high0 are similar but

without the contribution of q at initial time. The horizontal spectra of qmod0 at initial and final time are given in Fig. 9(c). Compared with horizontal spectra of extratropical SVs there is still the up-scale cascade of energy during the two-day integrations but there is more energy towards larger scales at initial time (SVs of type high0 give similar results). The stream-function fields of the three leading SVs of qmod0 are given in Fig. 10 at model level 18 (500 hPa). Notice that most of the amplitude is now confined to 30°S–30°N. We studied whether the SVs for qmod0 could be retained when cumulus convection was switched off in the linear models. The similarity index of 0.64 between the two subspaces consisting of 15 SVs shows that this diabatic process substantially contributes to the structures of the leading SVs.

In the preceding we have seen that spurious shallow SVs in the upper troposphere produced by barotropic and/or inertial instability could be prevented from growing through an increased vertical diffusion in the linearized model. Large values of specific humidity at initial time around 150 hPa have been reduced by replacing the q term in the moist TE-norm by a term based on background-error statistics. Also, mid-latitude SVs can be captured if the tropical area is not restricted enough. These properties of tropical SVs have been useful to design a set-up of targeted SVs for tropical cyclones presented in the next section.

5. Singular vectors targeted for tropical cyclones

As an application of tropical SVs, two tropical cyclones, Bonnie and Zeb, were studied, with starting dates 12 UTC 19 August 1998 and 12 UTC 11 October 1998 respectively. The purpose of this section is to define an SV configuration which yields structures associated with perturbation growth near cyclones. Such SVs may then be used in ensemble forecasting to provide information on, for example, uncertainties of the cyclone track. The impact of such SVs on the ECMWF EPS is the subject of a companion paper (Puri *et al.* 2001). Various SV configurations were tried, varying the choice of final norm and target area. Selecting a target area in the vicinity of the forecast cyclone track up to optimization time makes it more likely that SVs are associated with cyclone development. Target areas used for Bonnie and Zeb were, for example, 10°N–30°N, 80°W–60°W and 0°N–30°N, 110°E–140°E respectively. As noted in section 4(a), SV computations without increased vertical diffusion lead to SVs with spuriously large perturbation growth in the upper troposphere. This also appeared to be the case for the targeted SVs. Increasing the vertical diffusion as before could not entirely prevent the occurrence of the shallow SVs. Since perturbation growth for these SVs is only confined to a few model levels, targeted SV computations were performed with a final norm set to zero above model level 18 (500 hPa) but without increased vertical diffusion. This approach is efficient in excluding shallow upper-tropospheric SVs, because such structures then have a zero norm and are therefore not selected in the SV computation. Similarity indices based on 25 initial SVs with the dry TE-norm showed a good correspondence with the SVs obtained with the increased vertical diffusion setting high0 (0.76 and 0.79 for Bonnie and Zeb respectively). Differences due to the use of simplified or new physics in the linear models became noticeable in nonlinear integrations of SVs: those computed with new linearized physics produced larger perturbation growth when integrated nonlinearly (not shown). This may partly explain why new physics SVs when applied in ensemble forecasting produce larger spread in cyclone-track positions than SVs using simplified physics (see Puri *et al.* 2001). The SV computations reported hereafter use new physics in the linear models together with the vertically capped final

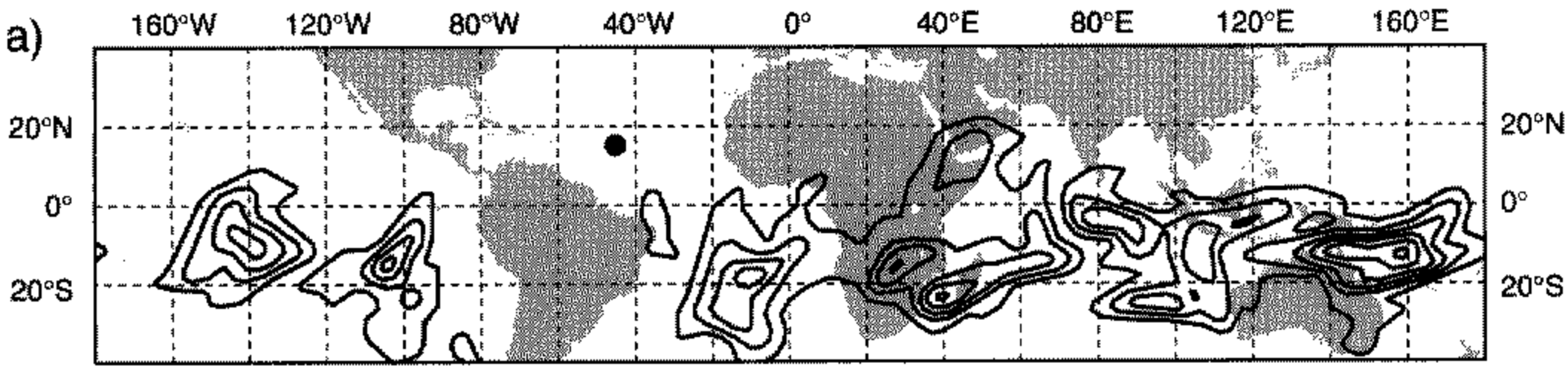

Figure 11. Stream-function root-mean-square fields at 500 hPa of the leading 25 singular vectors for tropical cyclone Bonnie and targeted for (a) 20°S–20°N and (b) 30°S–30°N; (c) and (d) same as (a) and (b) but for tropical cyclone Zeb. In all panels, the cyclone location is indicated by a large dot.

TE-norm and only the dry version. Including the specific humidity q term in the TE-norm at final time again resulted predominantly in SVs with all energy in q at final time, as with SV computations of type high1 or qmod1. This may be useful for particular studies, but when interested in a general probability forecast also for other components, such as temperature or wind, these type of SVs are not optimal. Therefore it was decided to omit the q term from the TE-norm.

The choice of the target area is crucial in determining the locations and properties of SVs (see also section 4(c)). Selecting as a target area the whole tropical strip 20°S–20°N resulted in many SVs which were not located in the cyclone area: similarity with the SV with the smaller target area around the cyclone position (see above) and based on the first 25 initial SVs was only 0.05 and 0.01 for Zeb and Bonnie respectively. Only SV12 and SV13 for the Zeb case and computed with the 20°S–20°N target area

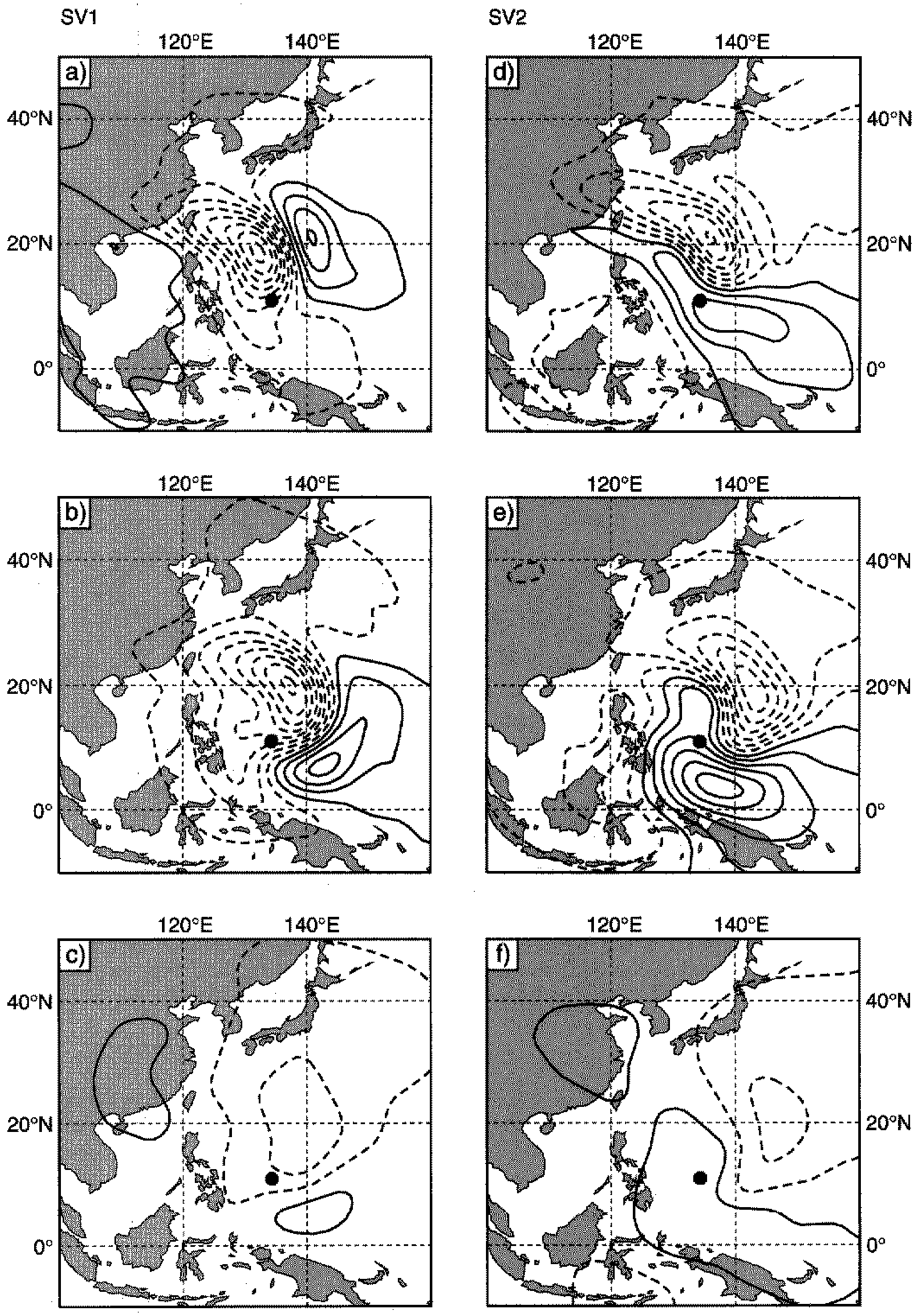

Figure 12. Stream-function fields of the two leading singular vectors (SVs) for tropical cyclone Zeb at three model levels (a) and (d) 270 hPa, (b) and (e) 500 hPa and (c) and (f) 770 hPa. The cyclone location is indicated by a large dot and negative values are shown dashed.

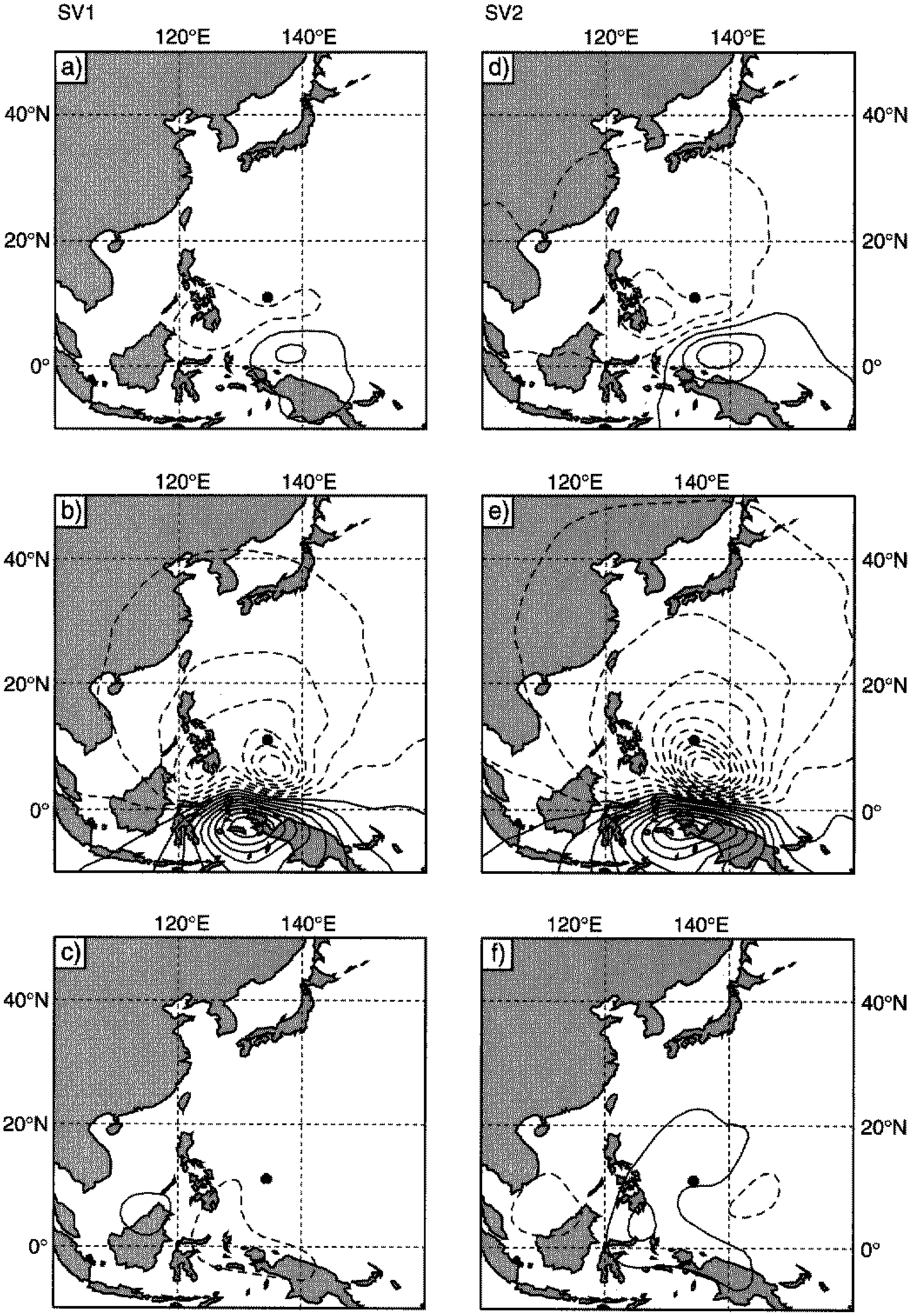

Figure 13. Same as Fig. 12 but for SV1 and SV2 computed with simplified physics.

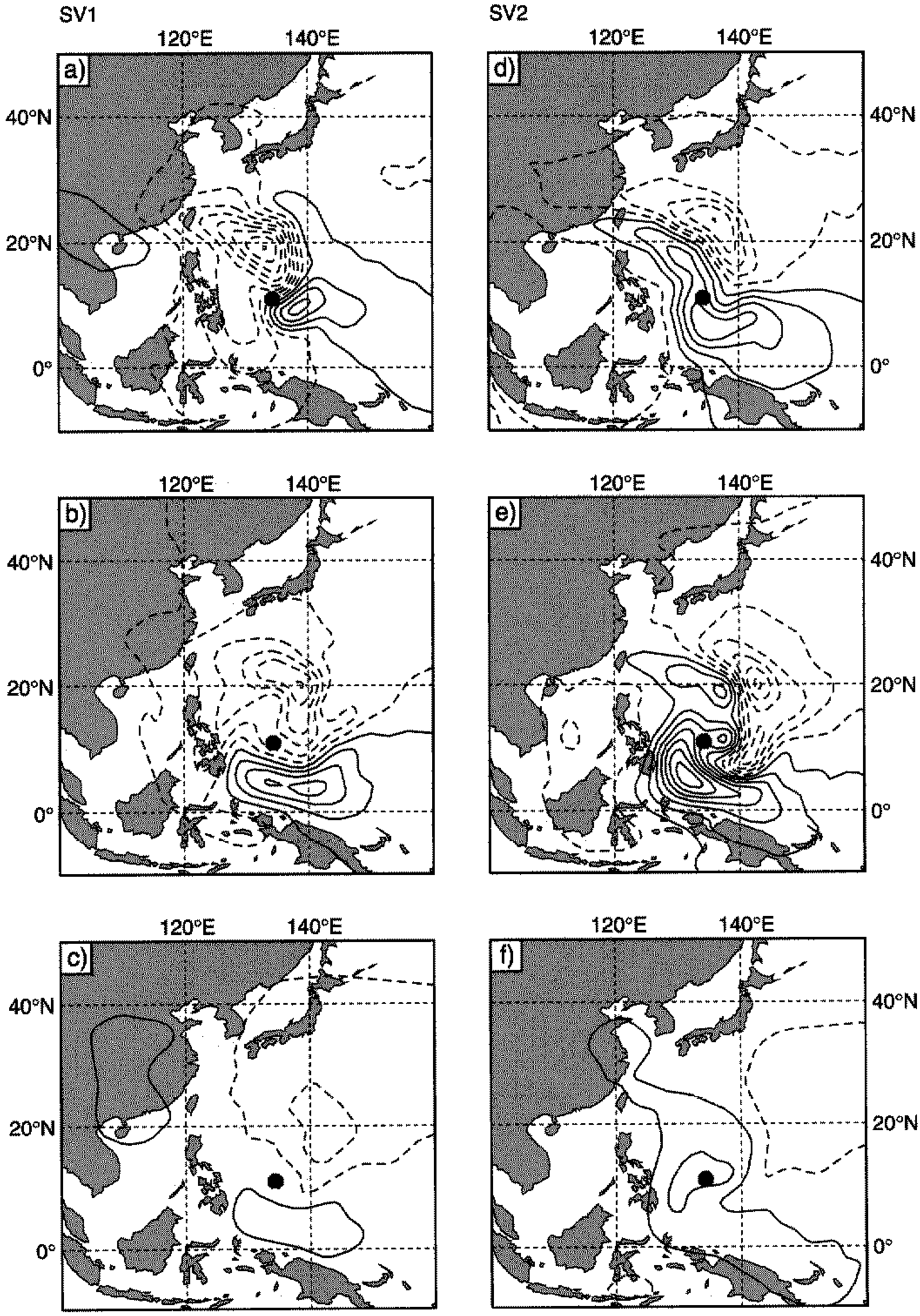

Figure 14. Same as Fig. 12 but for SV1 and SV2 computed at truncation T63.

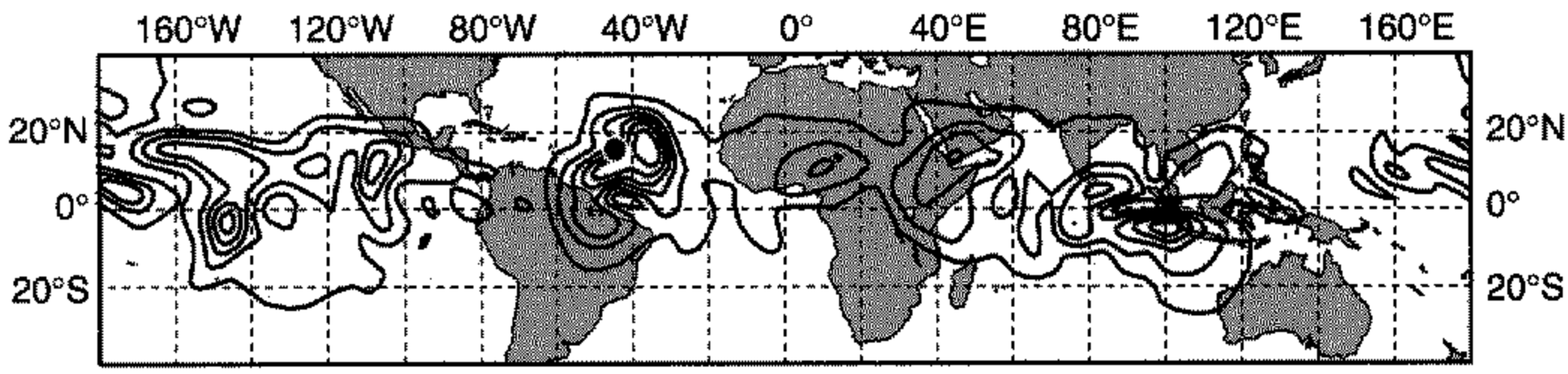

Figure 15. Stream-function root-mean-square field at 500 hPa of the leading 25 singular vectors for tropical cyclone Bonnie and targeted for 0°N–20°N. The cyclone location is indicated by a large dot.

had some projection on SV2 of the SVs computed for the smaller target area 0°N–30°N, 110°–140°E. The SVs computed with a target area 30°S–30°N even resulted in smaller similarity indices. Figure 11 shows the SV locations at initial time for Bonnie and Zeb and both tropical strip target areas as given by the stream-function root-mean-square fields of the leading 25 SVs. This critical dependence of the SV location on the target area shows that if tropical SVs are considered for hurricane ensemble prediction in an operational environment, the target area should be chosen with some care. To explore the sensitivity of SVs to the target area we therefore also determined SVs by targeting on the area where cyclones are likely to occur. For the Atlantic and Pacific regions the selected target areas are 100°W–0°W, 0°N–30°N and 100°E–220°E, 0°N–30°N respectively. Similarity indices of 0.68 and 0.77 between the smaller target area and the Atlantic and Pacific (based on 25 SVs) regions show that the unstable subspace has changed. However, the impact of both sets on the ensemble performance is quite similar, see Puri *et al.* (2001).

Figure 12 shows the two leading SVs at three model levels for a T42 computation using the smaller target area 0°N–30°N, 110°E–140°E for Zeb. Both SVs have substantial vertical structure, and horizontally most of the amplitude is in the vicinity of the cyclone position. This is in contrast with the T42 computation for the same target area but with simplified physics as is currently used in the ECMWF EPS, see Fig. 13. Although there is some amplitude at the lower and higher model levels, most of the amplitude is around 500 hPa. Also, the SV locations seem not to be associated with the cyclone position. Figure 14 shows the two leading T63 SVs of the same type as in Fig. 12. Clearly, there are similarities between the two sets (similarity indices based on 25 SVs are 0.53 and 0.65 for Bonnie and Zeb respectively). It is worth pointing out that, in particular, the leading T63 SVs show resemblance to spiraling optimal perturbations found by Nolan and Farrell (1999) for idealized vortices. As shown earlier, a number of features, such as choice of a dry or moist norm, the extent of target area, simplified or diabatic physics, have a significant influence on the structure of SVs in the region of a cyclone. The impact of these features of SVs on tropical cyclone prediction using the ECMWF EPS is considered in the companion paper by Puri *et al.* (2001).

In the case of tropical cyclone Bonnie (19 August 1998), the need for targeting seems to be the result of a more unstable SH winter circulation. Computations with target area 30°S–30°N and 20°S–20°N, yield SVs which are mainly located in the SH, see Figs. 11(a) and (b). To see whether tropical cyclone Bonnie could be isolated as an important feature without unnecessarily restricting the SV location, the tropical strip 0°N–20°N was selected as the target area. Figure 15 shows the stream-function root-mean-square fields of the leading 25 SVs. Clearly all leading SVs are now predominantly located in the NH, and tropical cyclone Bonnie in the Atlantic area is now covered

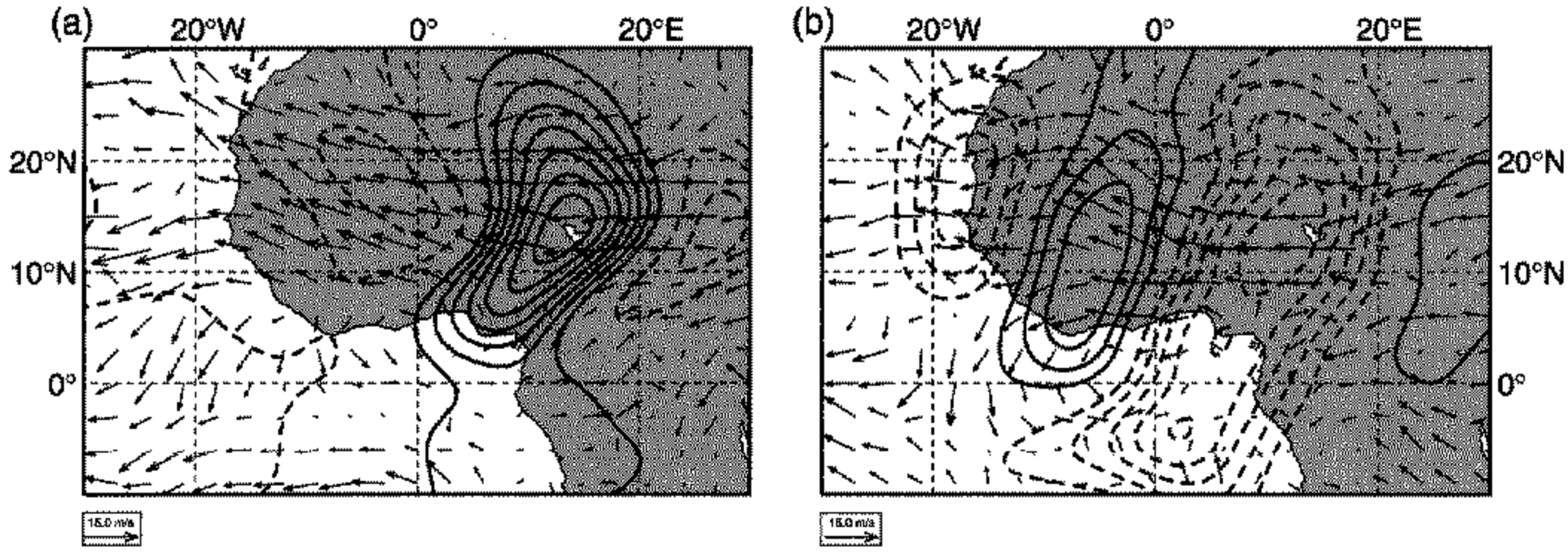

Figure 16. Stream-function fields at 500 hPa of a westward-propagating singular vector at (a) initial and (b) final time, with the wind vector fields of the corresponding analyses. Contour interval used in (b) is a factor three larger than in (a). Negative values are shown dashed.

well by SVs. Observe also that other areas associated with perturbation growth are now selected by the SV computation such as the monsoon area in the north Indian Ocean and the western African area, where so-called easterly waves originate. Figure 16 shows an example of a westward-propagating SV at 500 hPa located over western Africa, together with the wind vector fields of the corresponding analyses.

6. Conclusions

The development of a set of linear physical parametrizations for the tangent-linear and adjoint model versions of the ECMWF global forecast model as described by Mahfouf (1999) makes it possible to compute SVs for situations where physical processes may play an important role in perturbation growth. In this study we focused on the tropical region and determined tropical SVs exploring different norm configurations. For instance, the impact of including specific humidity in generating perturbation growth was studied.

First experiments with the new set of linear parametrizations resulted in SVs which had very shallow structure. Similar SVs were found with the original tangent and adjoint model which only uses a simplified vertical diffusion scheme (Buizza 1994). Most of the energy was confined to a few (upper tropospheric) model levels and dominated by the vorticity and divergence. Moreover, the linear and nonlinear evolution of these SVs showed a large discrepancy between their spatial pattern and perturbation growth. There is indication that these SVs are caused by inertial instabilities which are allowed to amplify freely in the linear model. For this reason the standard setting for the pseudo height of the boundary layer and for the asymptotic mixing length in the free atmosphere were changed to increase the vertical diffusion in the linear models at higher model levels. This prevented the occurrence of these shallow SVs. Moreover, the linear and nonlinear SV integrations showed a better match. In the extratropics, where the perturbation growth is dominated by baroclinic processes, the SVs are not affected by the increased vertical diffusion.

For two tropical cyclone cases in 1998, namely Bonnie and Zeb, targeted SVs were determined in various configurations. Results show that the selection of a target area requires some care in order to pick up perturbation growth associated with cyclone evolution. In a companion paper (Puri *et al.* 2001), the impact of these targeted tropical SVs on the performance of the ECMWF EPS will be studied. One of the findings is that

including linearized diabatic physics in the SV computation has a noticeable impact on the spread of cyclone tracks.

ACKNOWLEDGEMENTS

Drs A. Simmons and M. Miller are thanked for giving comments on an earlier version of the manuscript. The reviews of two anonymous referees provided useful comments and suggestions.

REFERENCES

Barkmeijer, J., Gijzen, Van M. and Bouttier, F. 1998 Singular vectors and estimates of the analysis-error covariance metric. *Q. J. R. Meteorol. Soc.*, **124,** 1695–1713

Blackadar, A. K. 1962 The vertical distribution of wind and turbulent exchange in a neutral atmosphere. *J. Geophys. Res.*, **67,** 3095–3102

Buizza, R. 1994 Sensitivity of optimal unstable structures. *Q. J. R. Meteorol. Soc.*, **120,** 429–451

Buizza, R. and Palmer, T. N. 1995 The singular vector structure of the atmospheric general circulation. *J. Atmos. Sci.*, **52,** 1434–1456

Buizza, R., Palmer, T. N., Barkmeijer, J., Gelaro, R. and Mahfouf, J.-F. 1996 'Singular vectors, norms and large-scale condensation'. Pp. 50–52 in Conference on numerical weather prediction, Norfolk, Virginia. American Meteorological Society

Derber, J. and Bouttier, F. 1999 A reformulation of the background error covariance in the ECMWF global data assimilation system. *Tellus*, **51A,** 195–222

Ehrendorfer, M. and Tribbia, J. J. 1997 Optimal prediction of forecast error covariances through singular vectors. *J. Atmos. Sci.*, **54,** 286–313

Ehrendorfer, M., Errico, R. M. and Reader, K. D. 1999 Singular vector perturbation growth in a primitive-equation model with moist physics. *J. Atmos. Sci.*, **56,** 1627–1648

Errico, R. M. and Reader, K. D. 1999 An examination of the accuracy of the linearization of a mesoscale model with moist physics. *Q. J. R. Meteorol. Soc.*, **125,** 169–195

Gelaro, R., Buizza, R., Palmer, T. N. and Klinker, E. 1998 Sensitivity analysis of forecast errors and the construction of optimal perturbations using singular vectors. *J. Atmos. Sci.*, **55,** 1012–1037

Holton, J. R. 1992 *An introduction to dynamic meteorology.* International Geophysics Series, Vol. 23. Academic Press

Hunt, B. G. 1981 The maintenance of the zonal mean state of the upper atmosphere as represented in a three-dimensional general circulation model extending to 100 km. *J. Atmos. Sci.*, **38,** 2172–2186

Lorenz, E. N. 1965 A study of the predictability of a 28-variable atmospheric model. *Tellus*, **17,** 321–333

1982 Atmospheric predictability experiments with a large numerical model. *Tellus*, **34,** 505–513

Louis, J.-F., Tiedtke, M. and Geleyn, J.-F. 1982 'A short history of the operational PBL parametrization at ECMWF'. Pp. 59–79 in ECMWF Workshop on boundary layer parametrization, November 1981, ECMWF, Shinfield Park, Reading RG2 9AX, UK

Mahfouf, J.-F. 1999 Influence of physical processes on the tangent-linear approximation. *Tellus*, **51A,** 147–166

Mahfouf, J.-F. and Rabier, F. 1999 'The ECMWF operational implementation of four-dimensional variational assimilation. Part II: Experimental results with improved physics'. ECMWF Technical Memorandum No. 242. (Available from ECMWF, Shinfield Park, Reading RG2 9AX, UK.)

Mahfouf, J.-F., Buizza, R. and Errico, R. M. 1996 'Strategy for including physical processes in the ECMWF variational data assimilation system'. Pp. 595–632 in ECMWF Workshop on non-linear aspects of data assimilation, 9–11 September 1996, ECMWF, Shinfield Park, Reading RG2 9AX, UK

Molteni, F., Buizza, R., Palmer, T. N. and Petroliagis, T. 1996 The ECMWF ensemble prediction system: Methodology and validation. *Q. J. R. Meteorol. Soc.*, **122,** 73–119

Nolan, D. S. and Farrell, B. F. 1999 Generalized stability analyses of asymmetric disturbances in one- and two-celled vortices maintained by radial inflow. *J. Atmos. Sci.*, **56,** 1282–1307

Palmer, T. N., Gelaro, R., Barkmeijer, J. and Buizza, R. 1998 Singular vectors, metrics and adaptive observations. *J. Atmos. Sci.*, **55,** 633–653

Parlett, P. 1980 *The symmetric eigenvalue problem*. Series in computational mathematics. Prentice Hall, New Jersey, USA

Puri, K., Barkmeijer, J. and Palmer, T. N. 2001 Ensemble prediction of tropical cyclones using targeted diabatic singular vectors. *Q. J. R. Meteorol. Soc.*, **127,** 709–731

Rabier, F., Klinker, E., Courtier, P. and Hollingsowrth, A. 1996 Sensitivity of forecast errors to initial conditions. *Q. J. R. Meteorol. Soc.*, **122,** 121–150

Rabier, F., Mahfouf, J.-F., Fisher, M., Järvinen, H., Simmons, A., Andersson, E., Bouttier, F., Courtier, P., Hamrud, M., Haseler, J., Hollingsworth, A., Isaksen, L., Klinker, E., Saarinen, S., Temperton, C., Thépaut, J.-N., Undén, P. and Vasiljević, D. 1997 'Recent experimentation on 4D-Var and first results from a simplified Kalman filter'. ECMWF Technical Memorandum No. 240. (Available from ECMWF, Shinfield Park, Reading RG2 9AX, UK.)

Simmons, A. J., Mureau, R. and Petroliagis, T. 1995 Error growth and estimates of predictability from the ECMWF forecasting system. *Q. J. R. Meteorol. Soc.*, **121,** 1739–1771

Thépaut, J.-N. and Courtier, P. 1991 Four-dimensional variational data assimilation using the adjoint of a multilevel primitive-equation model. *Q. J. R. Meteorol. Soc.*, **117,** 1225–1254

Vukićević, T. and Errico, R. M. 1993 Linearization and adjoint of parametrized diabatic processes. *Tellus.*, **45A,** 493–510